Materials Chemistry and Physics 204 (2018) 361–372

Contents lists available at ScienceDirect

Materials Chemistry and Physics

journal homepage: www.elsevier.com/locate/matchemphys

Physicochemical and catalytic properties of Pd/MoO_3 prepared by the sonophotodeposition method

M. Kolodziej [a], E. Lalik [a], J.C. Colmenares [b], P. Lisowski [b], J. Gurgul [a], D. Duraczyńska [a], A. Drelinkiewicz [a, *]

[a] Jerzy Haber Institute of Catalysis and Surface Chemistry, Polish Academy of Sciences, Niezapominajek 8, 30-239 Kraków, Poland
[b] Institute of Physical Chemistry, Polish Academy of Sciences, Kasprzaka 44/52, 01-224 Warszawa, Poland

HIGHLIGHTS

- Preparation of Pd/MoO_3 sample by sonophotodeposition method.
- The effect of sonophotodeposition on hydrogen bronze formation process.
- Palladium nanoclusters formation during sonophotodeposition treatment.

GRAPHICAL ABSTRACT

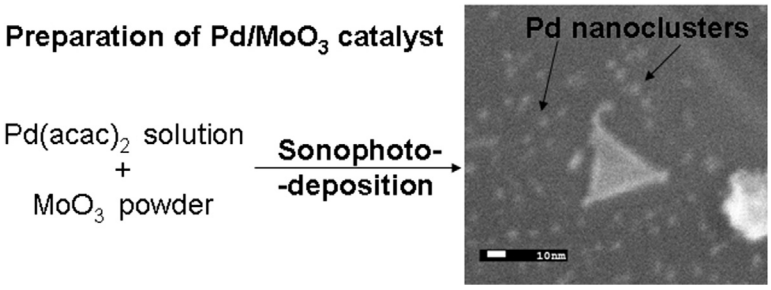

ARTICLE INFO

Article history:
Received 7 June 2017
Accepted 21 October 2017
Available online 26 October 2017

Keywords:
Palladium
Molybdenum trioxide
Sonophotodeposition
Cinnamaldehyde
Hydrogen bronze

ABSTRACT

Molybdenum trioxide-supported palladium catalyst Pd/MoO_3(SPD) is prepared by the sonophotodeposition procedure (SPD). This method combining sonication with ultraviolet irradiation is used at room temperature and atmospheric pressure and does not require the use of chemical reducing agent. For comparison, the Pd/MoO_3 catalysts are also prepared by the ultrasound irradiation and traditional impregnation - H_2 reduction methods. The Pd/MoO_3 catalysts are characterized by X-ray diffraction (XRD), electron microscopy (SEM, TEM, HRTEM), energy dispersive (EDS, STEM) analysis and X-ray photoelectron spectroscopy (XPS). The SPD treatment improves the platelets-like morphology of the MoO_3 oxide grains making more difficult formation of hydrogen bronzes H_XMoO_3 ($x > 0.9$) studied by microcalorimetric method. The "in situ" reduction of precursor ions during the SPD treatment generates much better dispersed Pd-nanoclusters than other preparation methods. It results in much higher activity of Pd/MoO_3(SPD) catalyst for the cinnamaldehyde hydrogenation than its MoO_3-supported counterparts and Pd/SiO_2, a reference catalyst.

1. Introduction

Molybdenum trioxide and polymolybdates are highly important compounds in catalysis. They could be applied as catalysts, catalysts precursors or supports for noble metals (Pt, Pd) - containing catalysts.

Upon high temperature treatment of MoO_3 with hydrogen, molybdenum bronzes H_XMoO_3 are generated which could be the precursors providing various types of catalytic active sites [1] The Mo-OH groups created in these structures could display catalytic activity via metallic as well as acid functions observed in

* Corresponding author.
E-mail address: ncdrelin@cyf-kr.edu.pl (A. Drelinkiewicz).

https://doi.org/10.1016/j.matchemphys.2017.10.060
0254-0584/

dehydrogenation and dehydration of propan-2-ol [2], isomerization of pentane, heptane [3], hydroisomerization reactions of linear C5-7 hydrocarbons [4,5]. Furthermore, hydrogen present in the bronze phases participated for the hydrogenation of unsaturated C=C bonds in alkenes [6,7]. Hydrogenation of ethylene on $H_{1.6}MoO_3$ formed in the Pt/MoO_3 catalyst proceeded without gaseous H_2 [7]. The DFT calculations for the ethylene - $H_XMoO_3(010)$ bronze system showed that the Mo-OH species could also participate in the adsorption of ethylene [8]. The interaction between protonic H of the Mo-OH group and π electrons of ethylene resulted in weak physisorption of ethylene in the tilted configuration which facilitated the transfer of hydrogen to the C=C bond. In our previous work similar effect has been observed in the hydrogenation of cinnamaldehyde (CAL), a reactant with C=C and C=O conjugated bonds on the Pd/MoO_3 catalysts [9]. The conditions of catalytic tests facilitating hydrogen bronzes formation promoted the hydrogenation of C=C bond of CAL reactant.

The MoO_3 has also been studied as the support for noble metal particles, such as Pt, Pd, etc. In catalytic reactivity of these systems, apart from the ability to hydrogen molybdenum bronzes formation also modification of electron properties of metal sites by the MoO_3 played a significant role. Zosimova et al. [10] reported that hydrogen species migration via spillover in the Pt/MoO_3 structure generated additional active sites active for toluene hydrogenation. Only those MoO_x particles that are in close vicinity to the Pt-particles took part in the formation of these additional active sites. An electron interaction between Pt, Pd particles and MoO_3 support is a well known effect [10–12]. Jackson et al. [12] reported that platinum in the Pt/MoO_3 sample was positively charged ($Pt^{\sigma+}$) due to metal –support interaction. The enhanced sulfur tolerance of Pt/MoO_3 catalysts has been also attributed to the electron deficient $Pt^{\sigma+}$ metal species [10,13].

Very low specific surface area of MoO_3 oxide (lower then 2 $m^2\ g^{-1}$) is a great disadvantage making difficult synthesis of catalysts with well dispersed metal (Pt, Pd) particles. Commonly used preparation method included impregnation of MoO_3 oxide with $PdCl_2/H_2PtCl_3$ aqueous solution followed by calcination (at 400 °C) or hydrogen reduction. However, the Pd-, Pt-MoO_3-supported catalysts with very low metal loading, 0.01–0.5 wt % were commonly obtained by this procedure [14–18]. For instance, the Pt/MoO_3 catalyst of as low metal loading as 0.1 mol % was studied for acrolein hydrogenation [14]. The metal loading in the MoO_3-supported catalysts studied for conversion of heptane and propanol-2-ol was also very low, 0.01 mol. % of Pt, Pd, Rh, Ir and Ru [15,16]. Preparation of Pt/MoO_3 catalysts by oxidation of Pt– Mo alloy precursors was more effective, as it produced catalysts of higher Pt loading but relatively large Pt particles 19–35 nm were formed [10]. Our previous studies showed that a colloid-based reverse "water-in-oil" microemulsion method produced the catalysts of high 2%Pd and 2%PdPt metal loading and uniform metal particles ca. 8–10 nm in size, but they aggregated to form large agglomerates [9,19]. The Pd/MoO_3 catalysts of 1–2 wt % Pd and much better dispersed Pd nanoparticles (ca. 8 nm) were formed when impregnation of MoO_3 was carried out using non aqueous medium, namely acetone solution of $Pd(ac)_2$ [9].

In the present paper a novel method of Pd/MoO_3 catalyst preparation is used, so called sonophotodeposition method (SPD). In this method sonication is combined with photocatalytic reduction of metal precursor ions carried out "in situ" [20–24]. This method is carried out at room temperature and atmospheric pressure and does not require the use of chemical reducing agent. The reducing agents are electrons produced as a result of the ultraviolet absorption by semiconducting material, MoO_3 oxide in our studies, while ultrasounds assure enhanced penetration of reagents in the support grains and help in the metal ions reduction. SPD method has already been effectively applied for the synthesis of various nanomaterials, among them several titania-based photocatalytic systems, Pd/TiO_2 [22,23] and bimetallic $PdAu/TiO_2$ ones [24]. Thus, present study focuses on preparation of MoO_3-supported palladium catalyst [Pd/MoO_3(SPD)] by the sonophotodeposition method. Physicochemical properties and catalytic reactivity of Pd/MoO_3(SPD) sample for the cinnamaldehyde hydrogenation are compared with those observed for the Pd/MoO_3 catalyst prepared by conventional impregnation - reduction method.

2. Experimental

2.1. Preparation of Pd-containing catalysts

Commercial molybdenum oxide (Johnson Matthey, surface area 1.7 m^2/g) was used as the supports. The 1.2%Pd/MoO_3(SPD) catalyst was prepared by sonophotodeposition procedure according to previously described procedure [22]. Shortly, 1 g of MoO_3 powder was dispersed in 120 cm^3 of H_2O: CH_3CN (30:70, v/v) solution consisting of 0.034 g of palladium(II) acetylacetonate and 0.1 g of oxalic acid. The preparation was carried out under argon flow (70 mL/min) at temperature of 20 °C. The suspension was first kept in dark for 30 min and then sonophotodeposition was performed by illuminating the suspension for 60 min with a low pressure mercury lamp (6 W, λ_{max} = 254 nm) and with ultrasonic bath (35 kHz, 560 W, Sonorex Digitec-RC, Bandelin) switched on. Then, the product was recovered by slowly evaporation in rotary evaporator, dried at 110 °C for 10 h, and calcined at 300 °C for 4 h under air flow (30 mL/min). For comparative purposes, a bare MoO_3 was also treated by the sonophotodeposition at palladium-free reaction medium (denoted as MoO_3(SPD)).

The 1%Pd/MoO_3(N) catalyst was prepared by impregnation of MoO_3 support with acetone solution of $Pd(ac)_2$ followed by reduction with hydrogen (5% H_2 in N_2) at temperature of 250 °C (3 h) [9].

2%Pd/SiO_2 (Silica Davisil 634, surface area 559 m^2/g) used as the reference catalyst was prepared as described before [9]. The synthesized catalysts were stored in contact with air.

2.2. Methods of characterization

The content of palladium (wt %) in the catalysts was determined by XRF method using Skaray Instrument EDX 3600H Alloy Analyzer.

The X-ray diffraction (XRD) patterns were obtained with a Philips X'PERT diffractometer using Cu Kα radiation (40 kV, 30 mA).

The X-ray Photoelectron Spectroscopy (XPS) measurements were carried out with a hemispherical analyzer (SES R4000, Gammadata Scienta). The unmonochromatized Al Kα and Mg Kα X-ray source with the anode operating at 12 kV and 20 mA current emission was applied to generate core excitation. All binding energy values were corrected to the carbon C 1s excitation at 285.0 eV. The samples were pressed into indium foil and mounted on a holder. All spectra were collected at pass energy of 100 eV except survey scans which were collected at pass energy of 200 eV. Intensities were estimated by calculating the integral of each peak, after subtraction of the Shirley-type background, and fitting the experimental curve with a combination of Gaussian and Lorentzian lines of variable proportions (70:30).

Electron Microscopy (SEM, TEM) studies were performed by means of Field Emission Scanning Electron Microscope JEOL JSM–7500 F equipped with the X-ray energy dispersive (EDS) system. Two detectors were used and the images were recorded in two modes. The secondary electron detector provided SEI images,

and back scattered electron detector provided BSE (COMPO) micrographs.

HRTEM and STEM studies were performed on FEI Tecnai G^2 transmission electron microscope operating at 200 kV equipped with EDAX EDX and HAADF/STEM detectors. Samples for analysis were prepared by placing a drop of the suspension of sample in ethanol or THF onto a carbon-coated copper grid, followed by evaporating the solvent.

Microcalorimetric experiments were performed using Microscal gas flow-through microcalorimeter. The instrument has been designed to measure thermal effects of solid/gas interactions concurrently with the gas uptake at constant temperature. The design as well as operation of the instrument has been previously described in detail [19,25]. The instrument design makes it possible to use in-situ calibration pulses of controlled power and duration, thus yielding a calibration factor for each individual experiment. The amount of evolving heat was monitored vs time, and concurrently the uptake of hydrogen was measured using thermoconductivity detector (TCD) located down-stream of the cell. The average molar heat (kJ/mol H_2) was calculated as a ratio of the total evolved heat and the total number of hydrogen moles consumed. The amount of the catalyst used to fill the microcalorimetric cell (ca. 0.15 cm^3) was ca. 0.2 g. The process of hydrogen sorption was carried out at temperature of 22 °C and under atmospheric pressure using 5% H_2 in N_2, flow rate 3 cm^3/min.

2.3. Hydrogenation reactions

Catalytic hydrogenation of cinnamaldehyde (CAL) was carried out in an agitated batch glass reactor at constant atmospheric pressure of hydrogen following the methodology previously described [9]. Toluene was used as the solvent. The catalyst was activated "in situ" prior to its contact with CAL-containing solution. After having been placed in reactor the dry sample of catalyst was wetted with toluene, and then activated by purging first with nitrogen (20 min; ambient temperature) and subsequently with hydrogen at temperature of 22 °C (15 min) and 50 °C (20 min).

The progress of the reaction was monitored by measuring the hydrogen consumed against reaction time. Samples of solutions were withdrawn from the reactor and analyzed using GC chromatograph PE Clarus 500, with FID detector and capillary column Elite-5 MS [9]. Typically, the hydrogenation test was carried out at 50° C using 20 cm^3 of CAL solution of $c^\circ = 0.05$ mol/dm^3 and catalyst concentration 5 g/dm^3.

Shaking of the reactor was carried out at such a speed to ensure that the rate of hydrogen uptake did not depend on agitation speed. External diffusion resistance was ruled out, since no significant variation in the catalytic results was observed by increasing the agitation speed.

3. Results and discussion

The ultrasound irradiation (sonication) is used routinely in the field of materials science, most frequently in order to accelerate chemical reactions. In the preparation of supported catalysts sonication is often coupled with traditional synthesis methods, like wet impregnation, sol-gel [20–22]. However, the ultrasound irradiation results in specific reaction conditions arising from a process called acoustic cavitation; the formation, growth and implosive collapse of the bubbles in a liquid, which produces unusual chemical and physical environments [26]. The extremely high temperatures, pressures and cooling rates attained locally during acoustic cavitation lead to many unique properties in the irradiated liquid system. Ultrasonic irradiation of liquid-powder suspensions can accelerate solid particles to high velocities and their collisions are capable of inducing dramatic changes in surface morphology, composition, like formation of new defects, enhancement of rates of intercalation in layered materials, fragmentation of brittle solids, agglomeration of metal powders. Chemical effect of ultrasound operation in liquids is the formation of free radicals, e.g. $H^{\cdot}$ and $OH^{\cdot}$. Then, they can recombine to form H_2O or interact to form H_2, H_2O_2 or HO_2. These radicals and compounds, with strong oxidative and reductive properties, are sources of various sonochemical processes in aqueous solutions [27]. The reduction of metal ions precursors, such as palladium or gold, to metal upon preparation of TiO_2-supported Pd or PdAu catalysts by SPD method has been related to the radicals sonochemically formed in aqueous solution [22–24].

Jeevanandam et al. [28] observed that sonication of polycrystalline MoO_3 particles suspended in *n*-decane resulted in some mechano-chemical changes. The morphology of MoO_3 particles was changed evidenced by distinct reduction of particle size. Besides, a partial reduction of Mo(VI) to Mo(V) occurred with subsequent introduction of shear defects attributed to the involvement of radicals generated in sonolysis of the solvent, *n*-decane. These changes were more pronounced when the ultrasound irradiation acted longer time, ca. 2–6 h. Tagaya et al. [29] also observed that the use of ultrasound irradiation essentially improved effectiveness of intercalation of alkylpyridines into the MoO_3 carrier.

In the present work, the sonophotodeposition procedure is used to prepare Pd/MoO_3(SPD) catalyst. The sample of initial MoO_3 is also treated by the sonophotodeposition procedure using palladium-free CH_3CN-water mixture. The sample of parent MoO_3 is also subjected to the sonication carried out for various periods of time (30–90 min) without the illumination stage. The ultrasound treated MoO_3 samples are subjected to the air calcination (350 °C for 2 h), e.g. similarly to the procedure of Pd/MO_3(SPD) catalyst preparation. Furthermore, the Pd/MoO_3(US) catalyst is synthesized using sonication only. For clarity, all the treatments used in the present work are listed in Table 1.

The sample of initial MoO_3 has very low surface area, 1.70 m^2/g which does not remarkably change for the SPD-treated parent MoO_3 oxide, 1.80 m^2/g. Incorporation of palladium results in slight decrease in specific surface area, to 1.50 m^2/g for the 1%Pd/MoO_3(SPD) catalyst.

Fig. 1 shows the XRD patterns of initial MoO_3 oxide and oxide samples treated by sonication [MoO_3(US)] and sonophotodeposition [MoO_3(SPD)] procedures. All the reflections in Fig. 1 are normalized by the most intense reflection at 2 θ = 25.75°. No amorphous background could be noticed, showing that no amorphous oxide is formed as a result of such treatments. As shown in Table 1, the lattice parameters of crystalline MoO_3 calculated for the bare MoO_3 and Pd/MoO_3(SPD) catalysts are close and they agree with the literature data [30]. The set of reflections registered in all the patterns does not essentially differ from that of initial MoO_3. The strong intensity of the reflections of (0*k*0) with k = 2, 4, and 6 proves the existence of the lamellar oxide structure in all the samples [30]. It can be seen that the intensity of two small reflections at 2 θ = 23.42° (peak B), and 2 θ = 27.31° (peak C) decreases relative to that of the most intense reflection at 2 θ = 25.75° (peak A). For clarity, the ratio of the line intensities A/B and A/C are calculated and collected in Table 1.

The intensity of B and C reflections decreases after air calcination of bare MoO_3 at 350 °C as well as after sonication for a short time (30 min) and becomes more pronounced after prolonged sonication, 90 min. The SPD treatment results in more dramatic changes evidenced by stronger reduction of both B and C reflections intensities. Similar decrease in the intensity can be seen in the XRD pattern of Pd/MoO_3(SPD) catalyst (Fig. 1). On the other hand, preparation of Pd/MoO_3(N) catalyst by traditional impregnation-reduction procedure does not induce the changes in the XRD

Table 1
Physicochemical properties of MoO_3 treated by various methods and Pd/MoO_3 catalysts prepared by various procedures.

Sample	Procedure	Surface area m^2/g	Pd content wt % (XRF)	XRD data, the ratio of intensity of reflections marked in Fig. 1	
				A/B	A/C
MoO_3	Initial a = 3.963 b = 13.860 c = 3.698 Å a = 3.962 b = 13.850 c = 3.697 Å[a]	1.70		5.6	5.9
	Calcination, 2 h 350 °C, air			14	14
	Calcination + sonication 30 min			10	10
	Calcination + sonication 90 min			11	12
	Sonitaction 30 min			8.4	9.8
	Sonication 90 min			12	13
	SPD	1.80		34	39
Pd/MoO_3	(N)	7.10	1	5.6	5.9
	(US)		0.4	4.3	5.0
	(SPD) a = 3.963 b = 13.859 c = 3.698 Å	1.50	1.2	13	17

[a] Literature data [30].

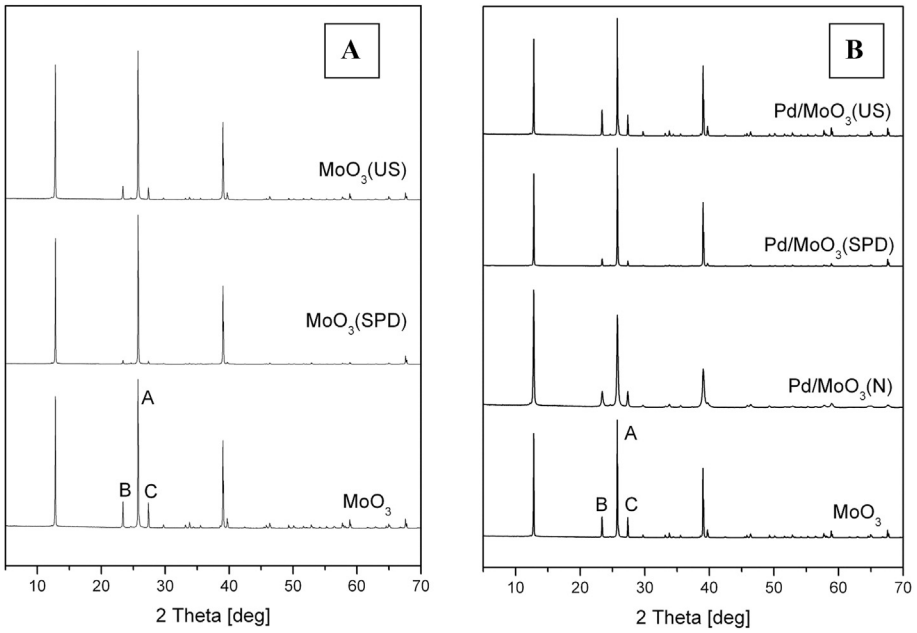

Fig. 1. XRD diffraction patterns (A) MoO_3 oxide and the samples treated by ultrasound irradiation MoO_3(US) and sonophotodepostion MoO_3(SPD) procedures; (B) MoO_3 - supported catalysts prepared by the impregnation-reduction Pd/MoO_3(N), sonophotodeposition Pd/MoO_3(SPD) and sonication Pd/MoO_3(US) procedure.

pattern. It is not clear why there are not changes in the XRD pattern of Pd/MoO_3(US) catalyst, whereas treatment of bare MoO_3 by sonication generated distinct changes.

Similar changes in the intensity of the reflections reported by Baiker et al. [31] have been ascribed to differences in morphology of the MoO_3 grains. In the XRD pattern of MoO_3 sample with well-developed platelets morphology and low surface area 0.05 m^2/g the reflection at 2 θ = 25.75° (040) strongly predominated. The intensity ratio of the reflections, corresponding to our A/C ratio, termed by the authors as the morphological factor was very high (ca. 60). On the other hand, such morphological factor was as low as 1 for the microcrystalline MoO_3 sample with small grains (1–2 μm), and higher surface area of ca. 5.5 m^2/g [31]. In view of these data, it might be suppose that sonication but especially SPD procedure, both treatments improved the platelets-like morphology of the oxide grains.

In Fig. 2, the representative SEM images of initial MoO_3 sample and after SPD treatment are displayed. The particles of well-developed platelet shape can be observed in both, initial and SPD-treated MoO_3 sample. This plate-like morphology is commonly related to unique layered structure of MoO_3. The comparison of micrographs registered at high magnification shows in the MoO_3(SPD) sample less distinct edges of plate-like grains. Jeevanandam et al. [28] observed distinct reduction of the grains size of polycrystalline MoO_3 after sonication in *n*-decane solvent. In these studies the time of sonication was definitively longer 6 h vs 1 h in our work, and experiment was carried out in *n*-decane solvent, whereas CH_3CN - water is used in the present work.

In Fig. 3 the FT-IR spectra of initial MoO_3, as-prepared and hydrogen treated Pd/MoO_3(SPD) catalysts are shown in the range 400–1050 cm^{-1}. The spectrum of hydrogen-treated catalyst is also provided, as the as-prepared catalyst is treated with H_2 prior to the catalytic hydrogenation experiments. Similarly to the literature data, the three main absorption patterns can be distinguish. The well defined and intensive band at ca. 990 cm^{-1} is attributed to the single-Mo-coordinated oxygen (Mo=O) stretching. An absorption pattern with two maxima at 870 and 821 cm^{-1} arise from the stretching vibrations in the Mo-*O*-Mo entity. A broad and complex bands in the spectral region 480 - 600 cm^{-1} are assigned to stretching plus bending vibrations of the Mo-*O*-Mo entity when

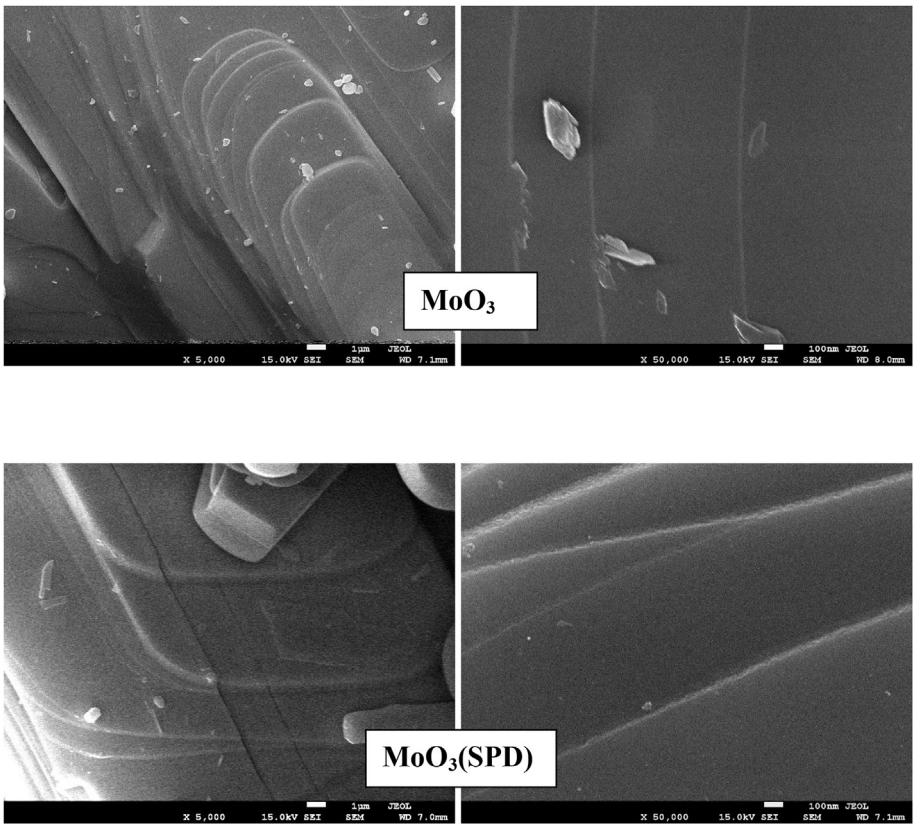

Fig. 2. SEM images of initial MoO_3 sample and after sonophotodeposition treatment.

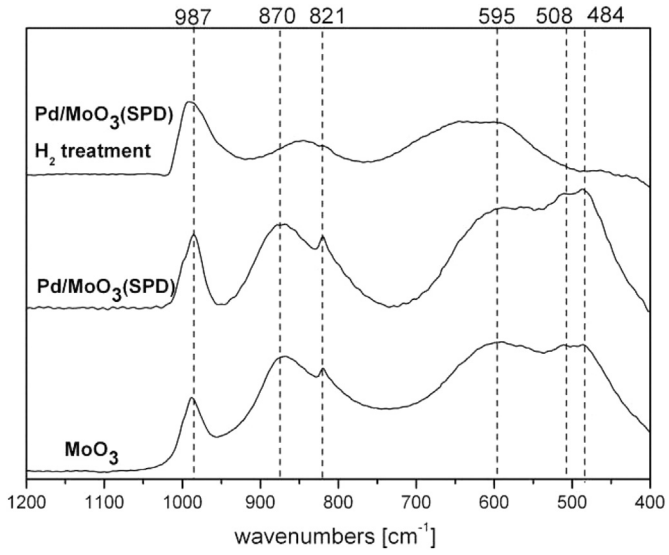

Fig. 3. FT-IR spectra of initial MoO_3, as-prepared and hydrogen treated (at 50 °C, 30 min) Pd/MoO_3(SPD) catalyst.

two axial oxygen atoms are common to two MoO_6 octahedra [32,33] It can be seen that the spectrum of Pd/MoO_3(SPD) catalyst does not remarkably differs form that of initial MoO_3 support. A small change of the shape and intensity ratio can be only seen in the range of 480–600 cm^{-1} ascribed to shear defects formation [28] However, prolonged (80 min) treatment of the Pd/MoO_3(SPD) catalyst with gaseous hydrogen at 50° C leads to quite different FT-IR spectrum, which is similar to the spectra for the hydrogen bronzes [32]. Thus, the observed changes associated with the formation of hydrogen bronzes in the Pd/MoO_3(SPD) catalyst prove that the SPD treatment does not reduce the ability of MoO_3 towards the formation of hydrogen bronzes.

The formation of hydrogen bronzes is also studied by the gas flow-through microcalorimetry measurements. This method makes it possible to measure the rate of heat evolution accompanying the sorption of hydrogen in the catalyst sample (Fig. 4).

The process of hydrogen bronzes formation is an exothermic reaction and the amount of evolved heat during the $H_{1.6}MoO_3$ bronze formation was reported to be 105 kJ/mol H_2 [1,19,34]. It should be noticed that incorporation of hydrogen into MoO_3 is much more exothermic than the hydrogen dissolution in the metallic Pd (ca. - 10.3 kJ/mol of $1/2H_2$ in a dilute H phase of Pd).

The result obtained for the Pd/MoO_3(SPD) catalyst are compared with that for the Pd/MoO_3(N) catalyst prepared by traditional impregnation-reduction procedure (Fig. 4). There is no essential difference in the shape of the hydrogen uptake and heat evolution curves. The amounts and the rates of heat evolution are very close on both catalysts up to the stoichiometry of ca. $H/MoO_3 = 0.9$. The rate of heat evolution during further hydrogen uptake corresponding to the bronze of $H/MoO_3 > 1$ is somewhat lower on Pd/MoO_3(SPD) catalyst than on the Pd/MoO_3(N) sample. However, total capacities of hydrogen incorporated are close for both Pd/MoO_3(SPD) and Pd/MoO_3(N) samples and correspond to the $H_{1.88}MoO_3$ stoichiometry. The formation of these bronzes is accompanied by similar amounts of evolved heat 89.3 and 90.2 kJ/mol for Pd/MoO_3(SPD) and Pd/MoO_3(N), respectively.

In the presence of Pt or Pd particles, the bronzes formation begins already at ambient temperature and is an extremely fast process providing a high degree of hydrogen incorporation [1,2,34]. The dissociation of H_2 on the Pt/Pd particles generates H atoms

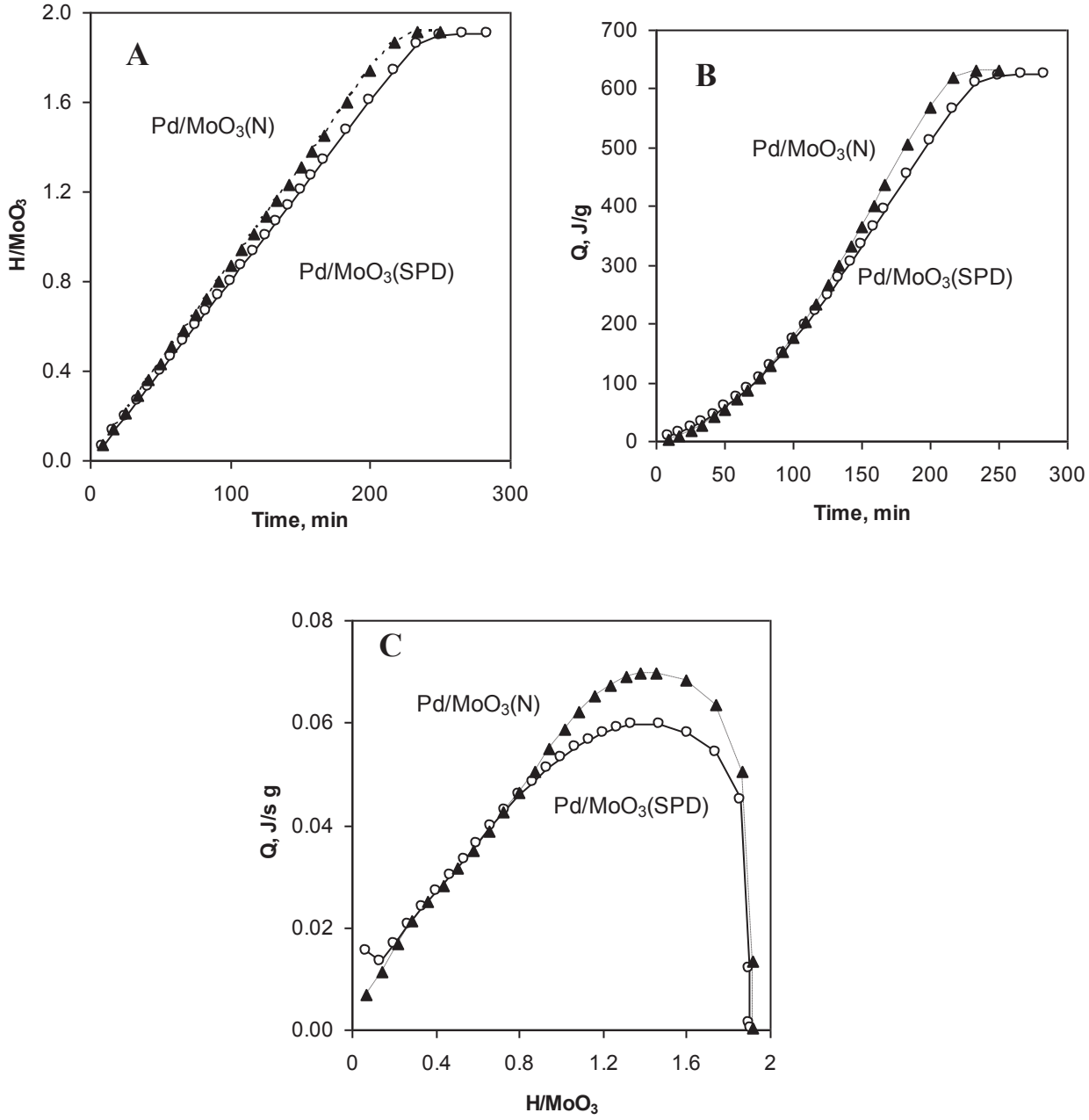

Fig. 4. Process of hydrogen bronzes formation in the Pd/MoO3(SPD) and Pd/MoO3(N) catalysts studied by micalorimetric method (temperature 22 °C, atmospheric pressure, gas flow rate 3 ml/min); (A) the obtained H/MoO_3 atomic ratio vs time of stream; (B) the amount of evolved heat (related to the 1 g of catalyst) vs time of stream; (C) the rate of heat evolution as a function of the hydrogen amount incorporated into the MoO_3.

which are highly mobile in the MoO_3 structure and migrate throughout the entire bulk solid by a spillover mechanism [35,36]. However, despites the experimental and theoretical studies, the exact locations of the H atoms in the bronze structures remain an open topic of research [37–41]. Ritter et al. [39] suggested that at low degree of hydrogen intercalation, H atoms first fill the intralayer position on the asymmetric bridging oxygen atoms which causes minor rearrangement. After saturation of these sites, for $x > 0.85$, the hydrogen starts to fill the interlayer positions coordinated with terminal oxygen atoms. A combined theoretical and experimental study suggested no hydrogen occupation on the intralayer sites, even at high H atom content $1.5 < x < 1.8$ [40]. DFT study reported by Chen et al. [41] revealed that at low coverage, the H atoms occupy preferentially asymmetrical (bridging) oxygen, whereas at high coverage they favorably reside on the terminal oxygen atoms which are the most favorable sites for accommodating two H atoms.

As shown in Fig. 4, there is no difference in the initial stage of hydrogen incorporation into the Pd/MoO_3(SPD) and Pd/MoO_3(N) samples. A difference is observed at high hydrogen content corresponding to $H/MoO_3 > 0.9$ making more difficult hydrogen incorporation in the case of SPD-treated sample. In view of the XRD diffraction pattern, the SPD procedure resulted in morphological changes improving the platelets-like morphology of the oxide grains. It might be suppose from these results, that morphology of the MoO_3 grains plays a role when high content of hydrogen is incorporated and microcrystalline morphology of the MoO_3 oxide as in the Pd/MoO_3(N) sample facilitates the hydrogen incorporation process.

The 2θ regions (35 - 50°) of XRD diffraction characteristic of Pd crystallites in all three Pd/MoO_3 catalysts are reported in supporting data (Fig. S1). The XRD pattern of Pd/SiO_2 catalyst presents the diffractions at 2θ ~40.08° and 46.71° corresponding to the (111) and (200) planes of crystalline Pd. From the Pd(111) line the average size of the Pd crystallites was calculated to be 8 nm [9]. A set of strong reflections of MoO_3 and especially the one at 2θ region of 39 - 40° makes it difficult an observation of the Pd reflection in Pd/MoO_3 (Fig. 1). No reflections originating from lower oxides like MoO_2 phase (2θ = 26, 36.9, 53.7°) can be seen in the XRD patterns of MoO_3 - supported catalysts calcined at temperature of 300 °C, consistent with previous reports for Pt/MoO_3 [1] and Pd/MoO_3 samples [42].

Electron microscopy (SEM, HRTEM) images of Pd/MoO_3(SPD) catalyst (Fig. 5) show Pd particles of size within wide range, from a few nanometers up to ca. 30 nm. Apart from a few aggregates of various shapes and sizes also individual relatively large Pd crystallites of tetrahedral shape appear. It should be stressed that palladium nanocrystals of tetrahedral shape are very rarely observed. Their formation is less favorable because of much larger surface to volume ratio relative to that in crystallites of octahedron shape [43]. The tetrahedral Pd crystallites were also observed in previously studied Pd/MoO_3 catalysts prepared by impregnation-hydrogen reduction procedure [9]. The formation of tetrahedral Pd nanostructures has been related to facilitated palladium ions migration due to the layered MoO_3 morphology.

However, apart from relatively large Pd-crystallites also nearly evenly distributed very small “dots” of regular shape and size in some regions of the MoO_3 surface are observed. To gain more inside into the nature of the “dots” the EDS analysis was carried out in selected areas of the surface (Fig. 6). The analysis showed the presence of Pd in each of the studied area but the Pd/Mo ratios differ strongly. In the analyzed area consisting of large palladium particles the atomic Pd/Mo ratios are as high as 0.32 and 0.38 (p. 1 and 2) being much higher than the Pd/Mo atomic ratio of 0.0136 calculated from the nominal composition. In the analyzed areas consisting of small “white dots” (p. 4 and 5) the Pd/Mo ratios are lower compared to the nominal one. The analysis carried out in area without distinct “dots” also showed Pd (p. 6 and 7), but the Pd/Mo ratios are much lower (0.0024 and 0.0051) than the nominal one. Based on these results, we can conclude that palladium species are present on the whole surface of the Pd/MoO_3(SPD) catalyst. It seems that two different Pd forms can be distinguish. The one is represented by relatively large Pd crystallites, the other consists of much smaller Pd nanoclusters of few nm in size and most of them is well and homogeneously distributed through the surface. These nanoclusters are also observed in HRTEM images of Pd/MoO_3(SPD) (Fig. 5).

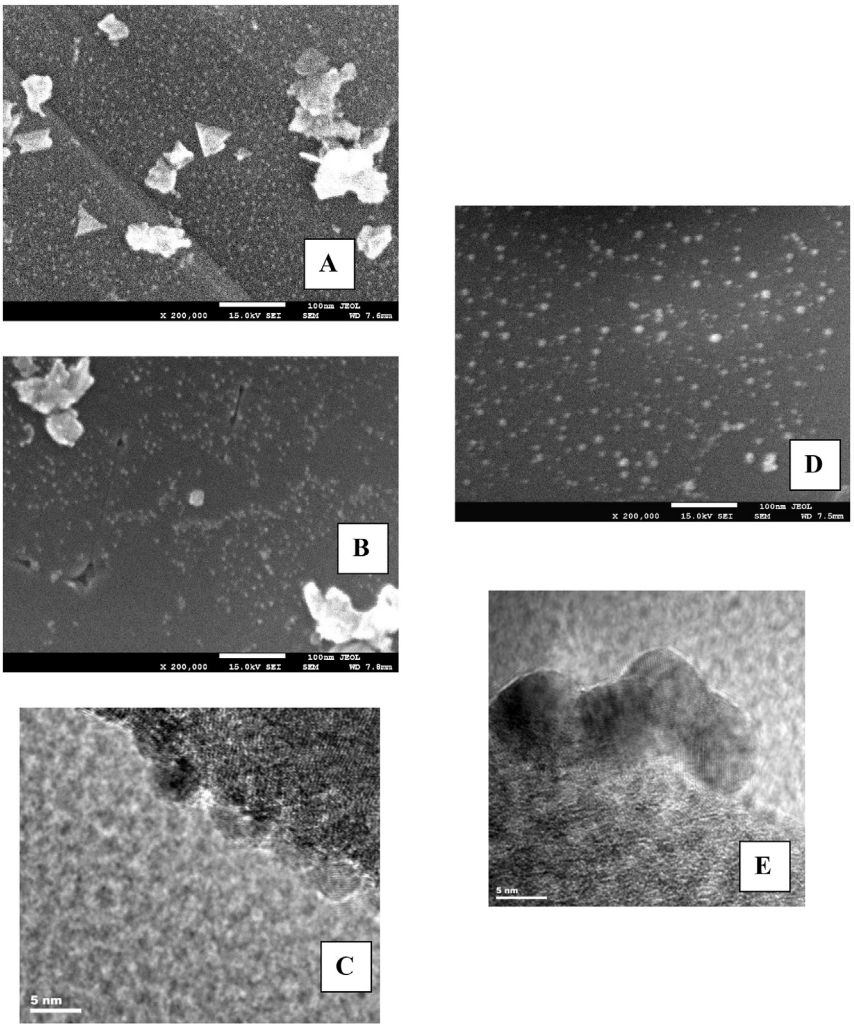

Fig. 5. SEM and HRTEM images of Pd/MoO_3(SPD) (A, B, C) and $PdMoO_3$(N) (D, E) catalysts.

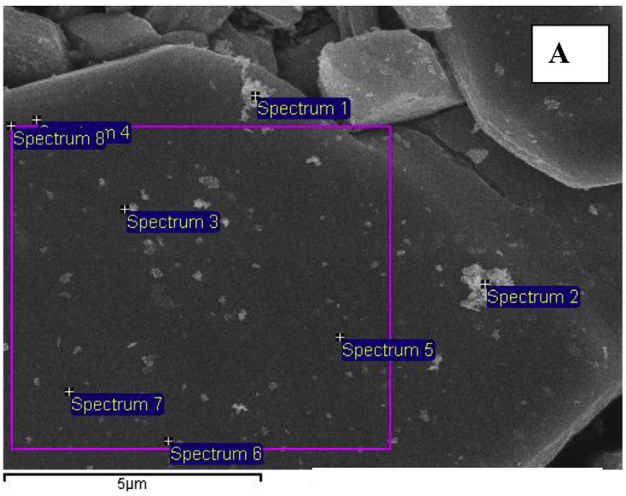

	Mo at %	Pd at %	Pd/Mo
1	18.10	5.86	0.32
2	18.32	6.97	0.38
3	25.66	0.67	0.026
4	24.15	0.33	0.012
5	26.32	0.31	0.012
6	24.85	0.06	0.0024
7	25.68	0.13	0.0051
8	26.59	0.09	0.0034

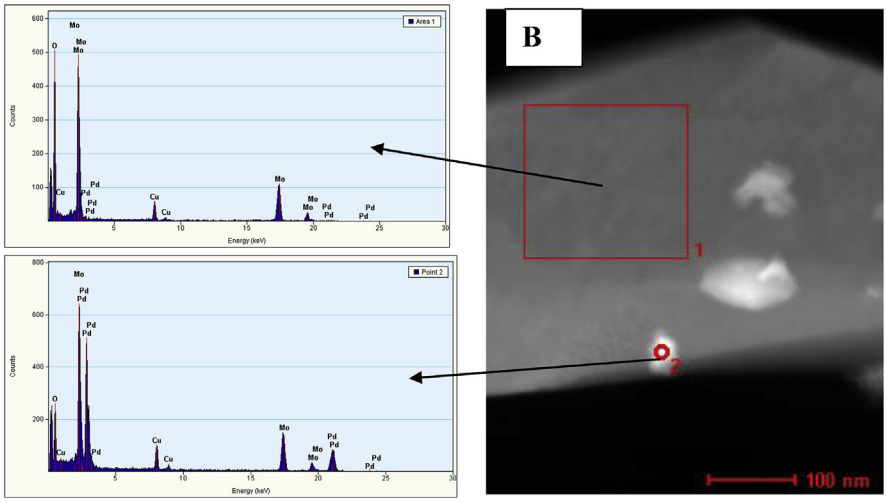

Fig. 6. Pd/MoO_3(SPD) catalyst; (A) SEM image and concentration of Pd and Mo (in at %) determined by EDS analysis; (B) STEM image and the EDX profiles.

The Pd particles of almost uniform size 6–8 nm located mostly on the surface of MoO_3-plates were observed in the Pd/MoO_3 catalysts prepared by traditional impregnation-reduction procedure [9]. Some aggregates composed of a few nanoparticles also existed. This type of palladium morphology can be also seen in the micrograph of the Pd/MoO_3(N) catalyst (Fig. 5). Comparison of the results for Pd/MoO_3(SPD) and Pd/MoO_3(N) catalysts clearly indicates that SPD procedure promotes the formation of much smaller Pd-nanoclusters than the impregnation-reduction procedure.

When sonication was used to prepare the Pd/MoO_3(US) catalyst, the incorporation of palladium ions was incomplete resulting in the 0.4 wt % Pd only, instead of 1 wt %. The low Pd-lading makes difficult the SEM analysis. Nevertheless, several relatively large and irregularly shaped aggregates consisting of Pd particles randomly distributed on the MoO_3 oxide are observed in SEM micrograph of Pd/MoO_3(US) catalyst (Fig. S2).

The catalysts are also subjected to the X-ray photoelectron spectroscopy (XPS) measurements (Fig. 7, Table 2). In the XPS Mo $3d_{5/2}$ spectrum of initial MoO_3 the peak at binding energy of 233.11 eV commonly ascribed to Mo(VI) predominates (88%). The binding energy of Mo(VI) could be observed within the range 232.6–233.7 eV depending on the oxygen surrounding and coordination [44,45]. A small contribution of Mo $3d_{5/2}$ peak component of lower energy 231.34 eV indicates some amount of Mo-species of lower oxidation number [46]. In view of linear relation between the Mo 3d binding energy and the oxidation number of Mo state with a slope of 0.8 eV per oxidation state [46], the observed energy of 231.34 eV could be ascribed to the Mo(IV) species. The Mo(VI) state dominates also in the spectra of all three catalysts, accompanied by a small contribution of the Mo(IV). The energies of the Mo-states in the spectra of Pd-containing catalysts are slightly positively shifted (by ca. 0.1–0.2 eV) (Table 2, Fig. 7) compared to MoO_3 oxide, which could be considered as the result of palladium – molybdenum oxide electron interactions.

In all three catalysts two palladium states are detected. The first of lower Pd $3d_{5/2}$ energy ca. 335 eV is characteristic of metallic Pd. The second one at higher energy of 336.6–336.8 eV could be associated with palladium – molybdenum oxide electron interactions, consistent with previous reports [10–12]. The DFT calculations revealed a strong charge transfer effect in the Pd-, Pt-clusters/MoO_3 systems [47]. Pt and Pd donated electrons to the nearest Mo or O -atoms and in the vicinity of the Pt and Pd atoms, the surface structure of MoO_3 was slightly distorted [47]. However, the binding energies slightly above 336 eV might be also associated with partial oxidation of palladium particles surface.

As shown in Table 2, metallic Pd strongly predominates (86%) in

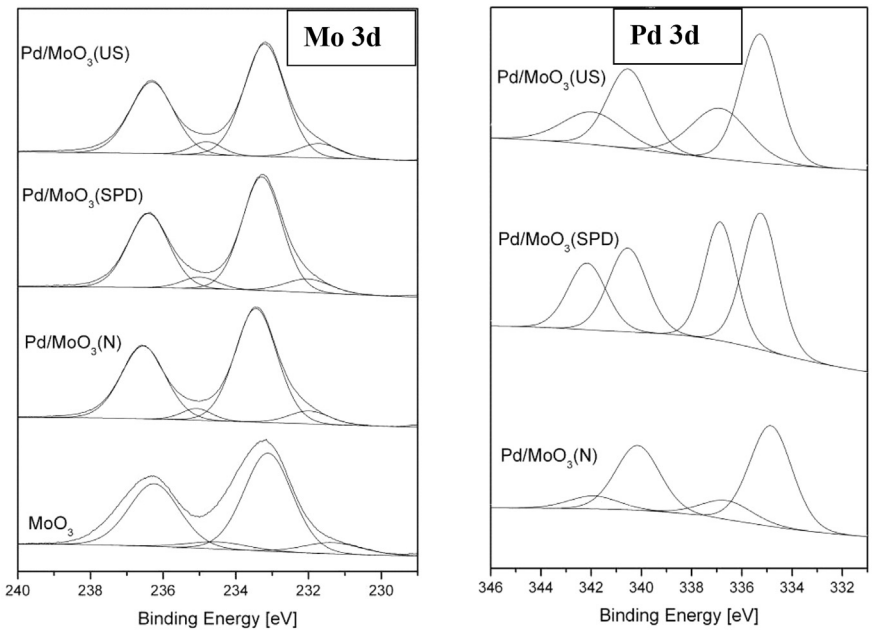

Fig. 7. XPS spectra of Mo 3d and Pd 3d regions for initial MoO_3 and MoO_3-supported catalysts prepared by impregnation - reduction Pd/MoO_3(N), sonophotodeposition Pd/MoO_3(SPD) and sonification Pd/MoO_3(US) procedure.

Table 2
Binding energy (eV) of Mo $3d_{5/2}$ and Pd $3d_{5/2}$ and contributions of peak components.

	Mo $3d_{5/2}$ (eV)		Pd $3d_{5/2}$ (eV)	
MoO_3	231.34	0.12		
	233.11	0.88		
0.4%Pd/MoO_3(US)	231.70	0.11	335.28	0.40
	233.21	0.89	336.88	0.60
1.2%Pd/MoO_3(SPD)	232.02	0.12	335.25	0.56
	233.29	0.88	336.86	0.44
1%Pd/MoO_3(N)	231.98	0.099	334.85	0.86
	233.45	0.90	336.61	0.14

the Pd/MoO_3(N) catalyst synthesized by impregnation - H_2 reduction procedure. The contributions of metallic Pd is lower in both catalysts prepared by US and SPD procedures, e.g. when reduction of palladium ions occurred due to sonochemical treatment without addition of reducing agents. In these catalysts, the contributions of metallic and ionic palladium species are comparable.

Catalytic results; hydrogenation of cinnamaldehyde (CAL)

In the present paper we focus on the activity of Pd/MoO_3 catalysts in the hydrogenation of cinnamaldehyde (CAL), an example of α,β-unsaturated aldehyde with a conjugated C=C and C=O bonds (Scheme 1). Hydrogenation of the former gives saturated aldehyde (hydrocinnamaldehyde, HCAL), the latter produces unsaturated alcohol (cinnamyl alcohol, COL) [48]. Apart from them, the fully saturated alcohol (HCOL) could be formed. Palladium is known to exhibit very high reactivity for the double C=C bond hydrogenation. Consequently, saturated aldehyde, (HCAL) is commonly formed as the dominating product on the Pd catalysts.

The selectivity of CAL hydrogenation is commonly related to the geometry of aldehyde adsorption on a metal surface [49,50]. A planar adsorption mode involving both C=C and C=O bonds favors hydrogenation of C=C yielding HCAL, while atop geometry involving the oxygen atom (C=O) promotes the formation of unsaturated alcohol (COL). The electron-deficient sites can act as an adsorption site for the C=O group of aldehyde thus improving the C=O selectivity. Promotion of C=O selectivity could be also attained using carriers like TiO_2, CeO_2, ascribed to the strong metal support interaction (SMSI) effect e.g. support-induced changes in reactivity of metal surface [51]. This effect observed for acrolein hydrogenation on the Pt/MoO_3 catalyst [14] has been related to electron-deficient sites created as a result of an association of platinum

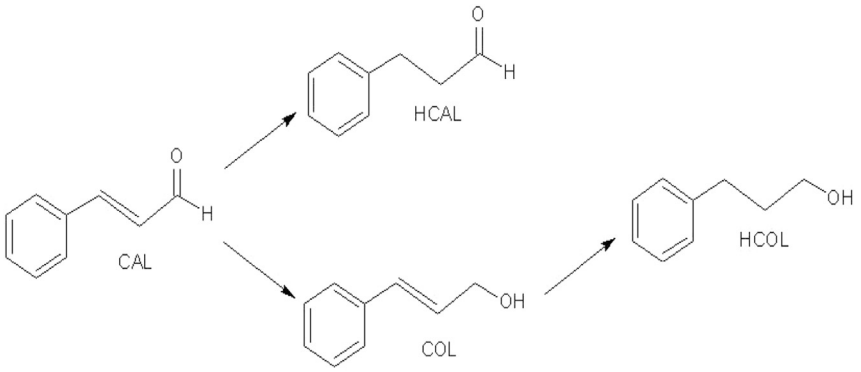

Scheme 1. Reaction pathways of cinnamaldehyde hydrogenation.

atoms and electron-deficient molybdena cations. These sites were generated during the reduction of Pt/MoO_3 catalyst with hydrogen at high temperature (300–400 °C).

The MoO_3 sample did not exhibit activity for CAL hydrogenation. In the presence of all studied catalysts, saturated aldehyde (HCAL) and saturated alcohol (HCOL) are observed from the very beginning of the reaction. No cinnamyl alcohol (COL) is detected at the present reaction conditions (toluene, 50 °C, atmospheric hydrogen pressure) consistent with previous results for Pd catalysts showing that all saturated alcohol (HCOL) is exclusively formed through the consecutive hydrogenation of the cinnamyl alcohol [48,52].

Fig. 8 a shows the decrease of CAL concentration against reaction time. The selectivity to C=C bond hydrogenation (formation of saturated aldehyde HCAL) against the conversion of CAL is plotted in Fig. 8 b. The catalytic properties of Pd/MoO_3 catalysts are compared with that of inert support-containing Pd/SiO_2 sample.

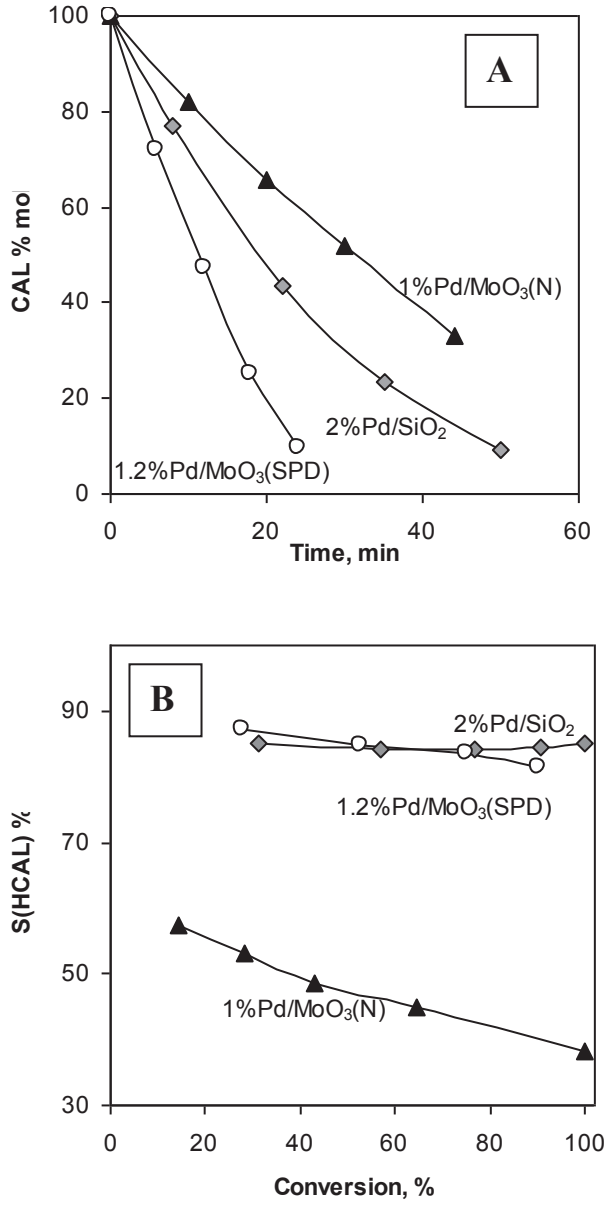

Fig. 8. Hydrogenation of cinnamaldehyde (CAL) over Pd/MoO_3(SPD), Pd/MoO_3(N) and Pd/SiO_2 catalysts; (A) decrease of CAL concentration against reaction time; (B) selectivity to saturated aldehyde (HCAL) formation against conversion of cinnamaldehyde. Reaction conditions: temp. 50 °C, catalyst concentration 5 g/dm^3, toluene solvent.

The Pd/MoO_3(US) catalyst exhibited very low activity, too low to be calculated. As shown in Fig. 8a, the Pd/MoO_3(SPD) catalyst is much more active than Pd/MoO_3(N) prepared by impregnation - reduction procedure. The initial rate normalized to the Pd mass on Pd/MoO_3(SPD) catalyst equal to 0.033 mol CAL/min g Pd is ca. 2-times higher than that on Pd/MoO_3(N) (0.015 mol CAL/min g Pd) and ca. 3-times compared to Pd/SiO_2 (0.012 mol CAL/min g Pd). The Pd/SiO_2 catalyst displays high selectivity to C=C hydrogenation, 85% (Fig. 8 b) which is preserved throughout the reaction. Similar and high selectivity is also attained on the Pd/MoO_3(SPD) catalyst. On the other hand, Pd/MoO_3(N) catalyst displays lower reactivity towards C=C hydrogenation evidenced by distinctly lower selectivity to HCAL, ca. 50–55%.

In typical procedure of catalytic tests, the catalyst is activated "in situ" by passing hydrogen (at 22 °C for 15 min and at 50 °C for 20 min) before the reaction. Under such hydrogen treatment the initially gray catalysts changed color due to hydrogen bronze formation. The color of Pd/MoO_3(N) catalyst changed to deep-blue whereas the Pd/MoO_3(SPD) sample was deep-red. The color was preserved during the whole hydrogenation experiment.

The formation of hydrogen bronzes is confirmed by XRD pattern registered for recovered 1%Pd/MoO_3(SPD) catalyst (after the catalytic experiment) (Fig. S3). For comparison, XRD diffraction of recovered Pd/MoO_3(N) catalyst is plotted. The samples of catalysts taken from the reactor were washed with acetone and dried in contact with air at room temperature. During this operation lasting ca. 0.5 h, a blue or deep-red color of the catalysts slowly vanished. Hydrogen bronzes are unstable in contact with air because of slow reoxidation to form the oxide phase [1]. The bronzes of high hydrogen content ($x > 1$) easily decompose whereas the oxidation is much more slower for the bronzes of H-content, below $x = 0.9$ [53,54]. In the XRD pattern of recovered Pd/MoO_3(SPD) catalyst (Fig. S3) there are no diffractions due to the MoO_3 phase, the reflections characteristic of $H_{0.34}MoO_3$ and $H_{0.9}MoO_3$ phases can be seen [16,55]. Hence, based on visually observed color of the samples it could be suppose that a high degree of hydrogen incorporation was attained in the catalysts during "in situ" activation by hydrogen.

It has been reported that hydrogen bronze ($H_{1.6}MoO_3$) formed in the Pt/MoO_3 catalyst acted as hydrogen reservoir for the ethylene hydrogenation as the formation of ethane proceeded due to the hydrogen arising from the bronze structure [7]. In these catalysts, the Pt particles played a double role; they are the gates by which the H atoms may leave the host lattice and Pt acted as the catalytic sites [8]. The DFT calculations showed that hydrogen on oxygen sites (Mo-O–H) of the bronze may activate ethylene via interaction with π electrons of the C=C bond [8]. A weak ethylene adsorption on the hydrogen bronzes makes it susceptible for attack from the nearby hydrogen-species only.

Our previous results showed that bronze phases formed in the Pd/MoO_3 catalysts could also provide active sites for the cinnamaldehyde hydrogenation via facilitated adsorption of CAL reactant in a planar adsorption mode favoring the C=C bond hydrogenation with consequently growing selectivity to saturated aldehyde (HCAL) [9]. Such activity/selectivity promotion manifested distinctly on catalyst with finely dispersed Pd nanoparticles. Therefore, high activity and enhanced selectivity to saturated aldehyde formation observed on the Pd/MoO_3(SPD) catalyst could result due to much better dispersed Pd metal evidenced by the Pd particles of smaller size compared to that in the Pd/MoO_3(N) catalyst prepared by impregnation-reduction procedure.

4. Conclusions

The sonophotodeposition procedure combining sonication with

ultraviolet irradiation proves to be effective method for incorporation of Pd nanoclusters into the MoO_3 oxide. The SPD treatment improves the platelets-like morphology of the MoO_3 oxide grains making more difficult incorporation of hydrogen upon formation of hydrogen bronzes H_XMoO_3 with high hydrogen content ($x > 0.9$). The "in situ" reduction of palladium ions during the SPD treatment generates well dispersed Pd-nanoclusters of smaller size compared to the Pd particles formed using traditional impregnation - hydrogen reduction preparation procedure. This found confirmation in catalytic properties of studied catalysts tested for the cinnamaldehyde hydrogenation. The Pd/MoO_3(SPD) catalyst has much higher activity than its MoO_3-supported counterparts and Pd/SiO_2 catalyst, a reference sample.

Appendix A. Supplementary data

Supplementary data related to this article can be found at https://doi.org/10.1016/j.matchemphys.2017.10.060.

References

[1] P.A. Sermon, G.C. Bond, Studies of hydrogen spillover. Part 1. Study of the rate, extent and products of hydrogen spillover from platinum to the trioxides of tungsten and molybdenum, J. Chem. Soc. Faraday Trans. I 72 (1976) 730–744.

[2] T. Matsuda, Y. Hirata, S. Suga, H. Sakagami, N. Takahashi, Effect of H_2 reduction on the catalytic properties of moltbdenum oxides for the conversions of heptane and 2-propanol, Appl. Catal. A 193 (2000) 185–193.

[3] T. Matsuda, H. Shiro, H. Sakagami, N. Takahashi, Isomerization of heptane on molybdenum oxides treated with hydrogen, Catal. Lett. 47 (1997) 99–103.

[4] S. Al-Kandari, H. Al-Kandari, A.M. Mohamed, F. Al-Kharafi, A. Katrib, Tailoring acid-metal functions in molybdenum oxides: catalytic and XPS-UPS, ISS characterization study, Appl. Catal. A 475 (2014) 497–502.

[5] H. Al-Kandari, A.M. Mohamed, S. Al-Kandari, F. Al-Kharafi, G.A. Mekhemer, M.I. Zaki, A. Katrib, Spectroscopic characterization-catalytic activity correlation of molybdena based catalysts, J. Mol. Catal. A 368–369 (2013) 1–8.

[6] P.A. Sermon, G.C. Bond, Studies of hydrogen spillover. Part 4. Factors affecting hydrogen spillover and its reversal, J. Chem. Soc. Faraday Trans. I 76 (1980) 889–900.

[7] J.P. Marcq, X. Wispenninkx, G. Poncelet, D. Keravis, J.J. Fripiat, Hydrogenation by hydrogen bronzes. Part I. Hydrogenation of ethylene by H_xMoO_3, J. Catal. 73 (1982) 309–328.

[8] M. Yang, B. Han, H. Cheng, First-principles study of hydrogenation of ethylene on a H_xMoO_3(010) surface, J. Phys. Chem. C 116 (2012) 24630–24638.

[9] M. Kolodziej, A. Drelinkiewicz, E. Lalik, J. Gurgul, D. Duraczynska, R. Kosydar, Activity/selectivity control in Pd/H_xMoO_3 catalyzed cinnamaldehyde hydrogenation, Appl. Catal. A 515 (2016) 60–71.

[10] P.A. Zosimova, A.V. Smirnov, S.N. Nesterenko, V.V. Yuschenko, W. Sinkler, J. Kocal, J. Holmgren, I.I. Ivanova, Synthesis, characterization, and sulfur tolerance of Pt-MoO_x catalysts prepared from Pt-Mo alloy precursors, J. Phys. Chem. C 111 (2007) 14790–14798.

[11] M.A. Pereira da Silva, R.A. Mello-Vieira, M. Schmal, Interaction between Pt and MoO_3 dispersed over alumina, Appl. Catal. A 190 (2000) 177–190.

[12] S.D. Jackson, J. Willis, G.D. McLellan, G. Webb, M.B.T. Keegan, R.B. Moyes, S. Simpson, P.B. Wells, R. Whyman, Supported metal catalysts: preparation, characterization and function. Part I. Preparation and physical characterization of platinum catalysts, J. Catal. 139 (1993) 191–206.

[13] R.M. Navarro, B. Pawelec, J.M. Trejo, R. Mariscal, J.L.G. Fierro, Hydrogenation of aromatics on sulfur-resistant PtPd bimetallic catalysts, J. Catal. 189 (2000) 184–194.

[14] C. Hoang-Van, O. Zegaoui, Studies of high surface area Pt/MoO_3 and Pt/WO_3 catalysts for selective hydrogenation reactions. Part II. Reactions of acrolein and allyl alcohol, Appl. Catal. A 164 (1997) 91–103.

[15] F. Uchijima, T. Takagi, H. Itoh, T. Matsuda, N. Takahashi, Catalytic properties of H_2-reduced MoO_3 with noble metal for the conversions of heptane and propan-2-ol, Phys. Chem. Chem. Phys. 2 (2000) 1077–1083.

[16] T. Matsuda, S. Uozumi, N. Takahashi, Effect of H_2 reduction on the catalytic properties of MoO_3 with noble metals for the conversions of pentane and propan-2-ol, Phys. Chem. Chem. Phys. 6 (2004) 665–672.

[17] S. Triwahyono, A. Abdul Jalil, S.N. Timmiati, N.N. Ruslan, H. Hattori, Kinetics study of hydrogen adsorption over Pt/MoO_3, Appl. Catal. A 372 (2010) 103–107.

[18] M. Susic, Y. Solonin, Kinetic-thermal processes of hydrogen sorption on Pd/WO_3 and Pd/MoO_3 bronze, J. Mater. Sci. 24 (1989) 3691–3698.

[19] E. Lalik, M. Kołodziej, R. Kosydar, T. Szumełda, A. Drelinkiewicz, Hydrogen and oxygen reaction on SiO_2 and MoO_3 supported Pd-Pt catalysts, Recycl. Catal. 2 (2015) 27–35.

[20] J.C. Colmenares, Ultrasound and Photochemical procedures for nanocatalysts preparation: application in photocatalytic biomass valorization, J. Nanosci. Nanotechnol. 13 (2013) 4787–4798.

[21] J.C. Colmenares, Sonication-induced pathways in the synthesis of light-active catalysts for photocatalytic oxidation of organic contaminants, ChemSusChem 7 (2014) 1512–1527.

[22] J.C. Colmenares, A. Magdziarz, D. Lomot, O. Chernyayeva, D. Lisovytskiy, A new photocatalytic tool in VOCs abatement: effective synergetic combination of sonication and light for the synthesis of monometallic palladium-containing TiO_2, Appl. Catal. B 147 (2014) 624–632.

[23] A. Magdziarz, J.C. Colmenares, In situ coupling of ultrasound to electro- and photo-deposition methods for materials synthesis, Molecules 22 (2017) 216–238.

[24] J.C. Colmenares, P. Lisowski, D. Łomot, O. Chernyayeva, D. Lisovytskiy, Sono-photodepositon of bimetallic photocatalysts $Pd\text{-}Au/TiO_2$: application to selective oxidation of methanol to methyl formate, ChemSusChem 8 (2015) 1676–1685.

[25] E. Lalik, R. Mirek, J. Rakoczy, A. Groszek, Microcalorymetric study of sorption of water and ethanol in zeolites 3A and 5A, Catal. Today 114 (2006) 242–247.

[26] A. Henglein, Sonochemistry: historical developments and modern aspects, Ultrasonics 25 (1987) 6–16;
(a) K.S. Suslick, S.J. Doktycz, E.B. Flint, On the origin of the sonoluminescence and sonochemistry, Ultrasonics 28 (1990) 280–290.

[27] J.H. Bang, K.S. Suslick, Application of ultrasound to the synthesis of nanostructured materials, Adv. Mater. 22 (2010) 1039–1059.

[28] P. Jeevanandam, Y. Diamant, M. Motiei, A. Gedanken, The effect of ultrasound irradiation on polycrystalline MoO_3, Phys. Chem. Chem. Phys. 3 (2001) 4107–4112.

[29] H. Tagaya, K. Takeshi, K. Ara, J. Kadokawa, M. Karasu, K. Chiba, Preparation of new organic-inorganic nanocomposite by intercalation of organic compounds into MoO_3 by ultrasound, Mater. Res. Bull. 30 (1995) 1161–1171.

[30] Q.P. Ding, H.B. Huang, J.H. Duan, J.F. Gong, S.G. Yang, X.N. Zhao, Y.W. Du, Molybdenum trioxide nanostructures prepared by thermal oxidation of molybdenum, J. Cryst. Growth 294 (2006) 304–308.

[31] A. Baiker, P. Dollenmeier, A. Reller, Influence of the grain morphology of molybdenum trioxide on its catalytic properties: reduction of nitric oxide with ammonia, J. Catal. 103 (1987) 394–398.

[32] K. Eda, Infrared Spectra of hydrogen molybdenum bronze $H_{0.34}MoO_3$, J. Solid State Chem. 83 (1989) 292–303.

[33] L. Seguin, M. Figlarz, R. Cavagnat, J.C. Lassegues, Infrared and Raman spectra of MoO_3 molybdenum trioxides and $MoO_3\ xH_2O$ molybdenum hydrates, Spectrochim. Acta Part A 51 (1995) 1323–1344.

[34] H. Noh, D. Wang, S. Luo, T.B. Flanagan, Y. Sakamoto, Hydrogen bronze formation within Pd/MoO_3 composites, J. Phys. Chem. B 108 (2004) 310–319.

[35] L. Chen, A.C. Cooper, G.P. Pez, H. Cheng, On the mechanism of hydrogen spillover in MoO_3, J. Phys. Chem. C 112 (2008) 1755–1758.

[36] X. Sha, L. Chen, A.C. Cooper, G.P. Pez, H. Cheng, Hydrogen absorption and diffusion in bulk α-MoO_3, J. Phys. Chem. C 113 (2009) 11399–11407.

[37] K. Eda, N. Sotani, Reexamination of protonic locations in hydrogen molybdenum bronze H_xMoO_3, J. Solid State Chem. 141 (1998) 255–261.

[38] J.J. Birtill, P.G. Dickens, Phase relationships in the system H_xMoO_3, Mater. Res. Bull. 13 (1978) 311–316.

[39] C. Ritter, W. Muller-Warmuth, R. Schollhorm, Structure and motion of hydrogen in molybdenum bronzes $HxMoO_3$ as studied by nuclear magnetic resonance, J. Chem. Phys. 83 (1985) 6130–6138.

[40] B. Braida, S. Adams, E. Canadell, Concerning the structure of hydrogen molybdenum bronze phase III. A combined theoretical-experimental study, Chem. Mater. 17 (2005) 5957–5969.

[41] Y.-H. Lei, Z.-X. Chen, DFT+U study of properties of MoO_3 and hydrogen adsorption on MoO_3(010), J. Phys. Chem. C 116 (2012) 25757–25764.

[42] T. Matsuda, F. Uchijima, S. Endo, N. Takahashi, Effect of Pd loading on the catalytic properties of molybdenum oxides for the isomerization of heptane, Appl. Catal. A 176 (1999) 91–99.

[43] Y. Wang, S. Xie, J. Liu, J. Park, ChZ. Huang, Y. Xia, Shape-controlled synthesis of palladium nanocrystals: a mechanistic understanding of the evolution from octahedrons to tetrahedrons, Nano Lett. 13 (2013) 2276–2281.

[44] R.I. Declerck-Grimee, P. Canesson, R.M. Friedman, J.J. Fripiat, Influence of reducing and sulfiding treatments on Co/Al_2O_3 and Mo/Al_2O_3 catalysts. An X-ray photoelectron spectroscopy study, J. Phys. Chem. 82 (1978) 885–888.

[45] A. Cimino, B. de Angelis, The application of X-ray photoelectron spectroscopy to the study of molybdenum oxides and supported molybdenum oxide catalysts, J. Catal. 36 (1975) 11–22.

[46] W. Grunert, A.Yu Stakheev, R. Feldhaus, K. Anders, E.S. Shpiro, K.M. Minachev, Analysis of Mo(3d) XPS spectra of supported Mo catalysts: an alternative approach, J. Phys. Chem. 95 (1991) 1323–1328.

[47] B. Li, W.-L. Yim, Q. Zhang, L. Chen, A comparative study of hydrogen spillover on Pd and Pt decorated MoO_3 (010) surfaces from first principles, J. Phys. Chem. C 114 (2010) 3052–3058.

[48] P. Gallezot, D. Richard, Selective hydrogenation of α,β-unsaturated aldehydes, Catal. Rev. Sci. Eng. 40 (1998) 81–126.

[49] F. Delbecq, P. Sautet, Competitive C=C and C=O adsorption of α,β-unsaturated aldehydes on Pt and Pd surfaces in relation with the selectivity of hydrogenation reactions: a theoretical approach, J. Catal. 152 (1995) 217–236.

[50] F. Delbecq, P. Sautet, A density functional study of adsorption structures of unsaturated aldehydes on Pt(111): a key factor for hydrogenation selectivity, J. Catal. 211 (2002) 398–406.

[51] P. Maki-Arvela, J. Hajek, T. Salmi, D.Yu. Murzin, Chemoselecitve hydrogenation of carbonyl compounds over heterogeneous catalysts, Appl. Catal. A 292

(2005) 1–49.
[52] A. Cabiac, T. Cacciaguerra, P. Trens, R. Durand, G. Delahay, A. Medevielle, D. Plee, B. Coq, Influence of textural properties of activated carbons on Pd/carbon catalysts synthesis for cinnamaldehyde hydrogenation, Appl. Catal. A 340 (2008) 229–235.
[53] N. Sotani, K. Eda, M. Kunimoto, Nuclear magnetic resonance and differential thermal analysis studies of hydrogen molybdenum bronzes, H_xMoO_3, J. Chem. Soc. Farady Trans. 86 (1990) 1583–1586.
[54] N. Sotani, K. Eda, M. Sadamatu, S. Takagi, Preparation and characterization of hydrogen molybdenum bronzes, H_xMoO_3, Bull. Chem. Soc. Jpn. 62 (1989) 903–907.
[55] T. Ohno, Z. Li, N. Sakai, H. Sakagami, N. Takahashi, T. Matsuda, Heptane isomerization over molybdenum oxides obtained by H_2 reduction of H_xMoO_3 with different hydrogen contents, Appl. Catal. A 389 (2010) 52–59.